Unraveling the daytime source of molecular chlorine in the extra-polar atmosphere

Xiang Peng[1], Tao Wang[1†,] Weihao Wang[1,3], A.R. Ravishankara[2], Christian George[4], Men Xia[1], Min Cai[5], Qinyi Li[6], Christian Mark Salvador[7], Chiho Lau[8], Xiaopu Lyu[1], Chunnan Poon[1], Abdelwahid Mellouki[5], Yujing Mu[9], Mattias Hallquist[7], Alfonso Saiz-Lopez[6], Hai Guo[1], Hartmut Herrmann[10], Chuan Yu[1,11], Jianing Dai[1], Yanan Wang[1], Xinke Wang[4], Alfred Yu[8], Kenneth Leung[8], Shuncheng Lee[1], and Jianmin Chen[12]

Affiliations:

[1] Department of Civil and Environmental Engineering, the Hong Kong Polytechnic University, Hong Kong, 999077, China.

[2] Departments of Atmospheric Science and Chemistry, Colorado State University, Fort Collins, CO, 80523, USA

[3] Hangzhou PuYu Technology Development Co., Ltd, Hangzhou, Zhejiang, 311300, China.

[4] Univ Lyon, Université Claude Bernard Lyon 1, CNRS, IRCELYON, Villeurbanne, 69626, France.

[5] Institut de Combustion, Aérothermique, Réactivité et Environnement (ICARE), CNRS/OSUC, 45071 Orléans, Cedex 2, France.

[6] Department of Atmospheric Chemistry and Climate, Institute of Physical Chemistry Rocasolano, CSIC, Madrid, 28006, Spain.

[7] Department of Chemistry and Molecular Biology, University of Gothenburg, 405 30, Gothenburg, Sweden.

[8] Air Science Group Environmental Protection Department, HKSAR, Hong Kong, 999077, China.

[9] Research Center for Eco-Environmental Sciences, Chinese Academy of Sciences, Beijing, 100085, China.

[10] Leibniz Institute for Tropospheric Research (TROPOS), Atmospheric Chemistry Department (ACD), 04318 Leipzig, Germany.

[11] Environment Research Institute, Shandong University, Qingdao, Shandong, 266237, China.

[12] Department of Environmental Science and Engineering, Fudan University, Institute of Atmospheric Sciences, Shanghai, 200433, China.

†Correspondence to Tao Wang (cetwang@polyu.edu.hk)

Abstract

Chlorine atoms (Cl) are highly reactive and can strongly influence atmospheric abundances of climate and air quality-relevant trace gases such as methane and ozone (O_3). Despite extensive research on molecular chlorine (Cl_2), an important Cl atom precursor, in the polar atmosphere, its sources in other regions are still poorly understood. Here we report unprecedented levels of daytime Cl_2 (up to 1 ppbv, the highest atmospheric concentration ever reported, with an average of ~400 pptv) in a coastal area in Hong Kong, indicating the presence of a large daytime source (Cl_2 ~2.7 pptv/s at noon) as the lifetime of Cl_2 is only ~7 minutes at noon. Field and laboratory results reveal that photolysis of particulate nitrate under acidic conditions (pH <3.0) can activate chloride and account for the observed daytime Cl_2 production. The high Cl_2 concentrations observed at the site increased the atmospheric oxidation rate of volatile organic compounds (VOCs) by 24 to 132%, RO_x radical by 4-27%, and daytime O_3 integrated production by 17%. Given the ubiquitous existence of chloride, nitrate, and acidic aerosols, we propose that nitrate photolysis is a significant daytime chlorine source globally. This so far unaccounted for a new source of chlorine can have substantial impacts on global atmospheric chemistry.

Article main text

Introduction

Atomic chlorine (Cl) is a very reactive radical, known to destroy stratospheric ozone (O_3) through catalytic cycles [1,2]. In the lower troposphere, it can initiate the oxidation of volatile organic compounds (VOCs), increase the levels of conventional radicals (OH, HO_2 and RO_2), and produce O_3 and secondary organic aerosols (SOA), which are air pollutants and also alter the Earth's radiation budget and climate [3-7]. Cl reacts rapidly with methane, the most abundant VOCs and the third-most important greenhouse gas in the atmosphere [8,9]. Molecular chlorine (Cl_2) is an important Cl precursor. It can be photolyzed quickly to release two Cl atoms during the daytime, and its production through heterogeneous reactions is a key step in the O_3 destruction over Antarctica during austral spring [10]. Previously, Cl_2 has been measured in the lower troposphere in locations such as at the Arctic surface [11], the marine boundary layer [12-14], and continental sites [15,16]. Cl_2 was found to typically peak during nighttime, but elevated levels (17-450 ppt) have also been observed during daytime [6,11,17-20]. The daytime occurrence of Cl_2 is of great importance as it may have a profound impact on atmospheric photochemistry and oxidation capacity [6,18]. Such observations also reveal the existence of a significant Cl_2 source that compensates or even overcomes its fast photolytic loss. Although daytime Cl_2 can be emitted from various sources, such as from coal combustion [15] or water treatment facilities [14], it can also be produced through some photochemical processes [11,17-19]. However, the underlying photochemical mechanisms remain uncertain. As a result, current state-of-the-art air quality models do not typically implement such chemistry, and therefore, cannot reproduce the observed high daytime Cl_2 levels in polluted regions [7,21]. Consequently, the impact of Cl_2 on atmospheric oxidation is currently underestimated.

To investigate the abundance, sources, and impact of Cl_2, we measured its concentrations using a chemical ionization mass spectrometer (CIMS) (Methods section 1) at a coastal site in southern China (22.21N, 114.25E, Fig. S1), adjacent to the highly industrialized Pearl River Delta (PRD). The field measurement took place from 31 August to 9 October 2018, when this site predominately received outflow of air from eastern and southern China and occasionally inflow of marine air and spillover of urban pollution from Hong Kong (HK) and other PRD cities [22,23] (see Methods section 2). Moderate to very high mixing ratios of ozone (up to 186 ppbv) (Fig. S2) were observed during the study, indicating active photochemistry during the measurement period.

We frequently observed Cl_2 mixing ratios greater than 400 pptv (10-min average) with a maximum of 998 pptv (Fig. S2), which is the highest value among the limited Cl_2 measurements reported to date in any location [6,9,18]. The Cl_2 mixing ratio exhibited a distinct daytime peak (Fig. 1A and Fig. S2), coinciding with that of ozone. Much higher Cl_2 levels were observed in the air mass originating from inland than that from the ocean, indicating the important role of anthropogenic pollution in producing the observed high Cl_2 (Fig. 1A, and Fig. 1B). The highest Cl_2 (and O_3) occurred on 11 September 2018 in a heavy photochemical pollution episode (Fig. S2), when the site was impacted by plumes from HK and other PRD cities [24]. With an average photolysis lifetime of Cl_2 of about 7-min at noon during this study, sustained high levels of daytime Cl_2 must arise from a significant in-situ production, with an average production rate of up to 2.7 pptv/s at noon. $ClNO_2$ - another Cl precursor - exhibited typical nighttime peaks with the highest mixing ratio of 1900 pptv, comparable to the value observed in our previous measurements at a nearby site [25].

Previous studies have proposed two chemical mechanisms to explain the observed daytime Cl_2 production. The first one involves the aqueous-phase reaction of OH with chloride in the solution or at the air-water interface, with OH being produced from O_3 photolysis in the gas or aqueous phase (R1 - R5) [26,27].

$$O_3 {}_{(g)} + h\nu \rightarrow O(^1D) {}_{(g)} + O_2 {}_{(g)} \tag{R1}$$

$$O(^1D) {}_{(g)} + H_2O \rightarrow 2OH_{(g)} \tag{R2}$$

$$OH {}_{(g)} + Cl^- {}_{(interface)} \rightarrow (OH...Cl^-)_{(interface)} \tag{R3}$$

$$OH {}_{(aq)} + Cl^- {}_{(aq)} \rightleftharpoons HOCl^-{}_{(aq)} \tag{R4}$$

$$2HOCl^- {}_{(aq\ or\ interface)} + 2H^+ {}_{(aq)} + 2Cl^- {}_{(aq)} \rightarrow Cl_2 {}_{(aq)} + 2Cl^- {}_{(aq)} + 2H_2O \tag{R5}$$
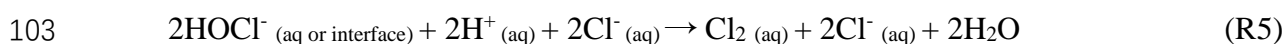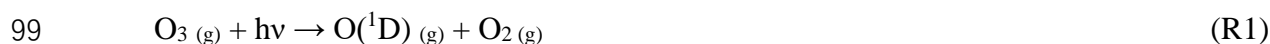
This mechanism was based on laboratory observations of the production of 10-100 ppb of Cl_2 when gaseous O_3 (0.8-14 ppm) and deliquesced sea salt particles were illuminated with 254 nm ultra-violet light [26]. The experimental results were supported by molecular dynamics and kinetics calculations [27]. These studies revealed a maximum Cl_2 production of 375 ppt s^{-1} (with 14 ppm O_3 and a photolysis rate constant for O_3 to generate $O(^1D)$ ($J(O_3 \rightarrow O(^1D))$ of 7.92×10^{-4} s^{-1}). If we extrapolate this production rate to our ambient conditions, i.e., O_3 (65 ppb) and $J(O_3 \rightarrow O(^1D))$ (1.78×10^{-5} s^{-1}), which is calculated from the TUV model under clear sky

111 condition, the O_3 photolysis would produce Cl_2 at a rate of 0.039 ppt s^{-1}, which is one order of
112 magnitude smaller than the average daytime (08:00-18:00) production rate (P(Cl_2)) of 0.46 ppt
113 s^{-1} measured at our site. Here the P(Cl_2) is assumed to be equal to the photolysis rate of Cl_2, as
114 the Cl_2 is nearly in a photo-stationary state (considering its short lifetime of ~7 min at noon in
115 our study).

116 Another suggested mechanism is the autocatalytic halogen activation, which begins with
117 a Cl atom reacting with O_3 to form chlorine monoxide (ClO) during daytime (R6 – R7). ClO
118 further reacts with HO_2 or NO_2 to form hypochlorous acid (HOCl) (R8) or chlorine nitrate
119 ($ClONO_2$) (R9), respectively. These two compounds can then undergo photolysis or react on
120 acidic chloride-containing aerosol particles to form Cl_2 (R10 – R11) that partitions to the gas
121 phase [9,28].

122 $$Cl_{2(g)} + hv \rightarrow 2Cl_{(g)} \tag{R6}$$

123 $$Cl_{(g)} + O_{3\ (g)} \rightarrow ClO_{(g)} + O_{2\ (g)} \tag{R7}$$

124 $$ClO_{(g)} + HO_{2\ (g)} \rightarrow HOCl_{(g)} + O_{2\ (g)} \tag{R8}$$

125 $$ClO_{(g)} + NO_{2\ (g)} + M \rightarrow ClONO_{2\ (g)} + M \tag{R9}$$

126 $$HOCl_{(g)} + H^+ + Cl^- \xrightarrow{aerosol} Cl_{2\ (g)} + H_2O_{(aq)} \tag{R10}$$

127 $$ClONO_{2\ (g)} + H^+ + Cl^- \xrightarrow{aerosol} Cl_{2\ (g)} + HNO_{3\ (aq)} \tag{R11}$$
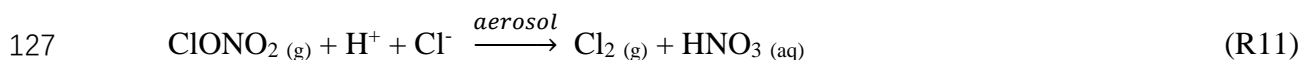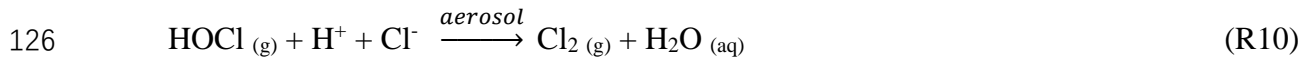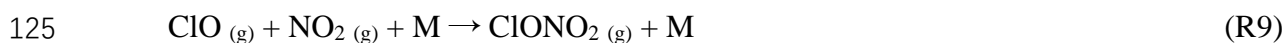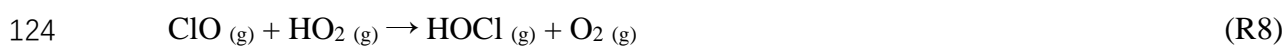
128 We used a photochemical box model [6] (also see Methods section 3) to simulate HOCl,
129 and $ClONO_2$ (Fig. S3) based on known gaseous chlorine chemistry, by constraining it to
130 observed Cl_2 and other chemical constituents concentrations (Supplementary Table. S1, and
131 Fig. S4). The calculations were performed for the period 4 - 14 September 2018, for which a
132 more complete VOC dataset is available. The simulated mixing ratios of HOCl were a factor
133 of 3 lower than those of Cl_2 (Fig. S3), as Cl atoms predominantly react with volatile organic
134 compounds (VOCs) (~83%) but less efficiently with ozone (~17%) to form ClO and then HOCl
135 at our site (see below). The calculated Cl_2 production rate (via R10) was two orders of
136 magnitude lower than the observed rate, even if we adopt the highest model-predicted HOCl
137 value (180 pptv) and previously reported the highest HOCl uptake coefficient of 0.0002
138 (Methods section 4), confirming the negligible role of HOCl in producing Cl_2 (via R10) at our
139 site. For $ClONO_2$, the model calculated mixing ratios (Fig. S3) were two orders of magnitude
140 lower than the observed Cl_2 values, suggesting its insignificant role in Cl_2 production (via R11).
141 To conclude, the previously two known mechanisms for producing daytime Cl_2 cannot account
142 for the high Cl_2 production observed, and the mismatch is over an order of magnitude.

143   To gain more insight into the potential sources of daytime Cl_2, we examined the
144 relationship between $P(Cl_2)$ and various measured parameters (Fig. S5) that might be involved
145 in the Cl_2 photochemical production. We found a good correlation between $P(Cl_2)$ and the
146 product of the solar actinic flux and the aerosol surface area density (R^2=0.71) (Fig. S5), and
147 the correlation was further improved with consideration of O_3 (R^2=0.91) (Fig. 1C) or nitrate in
148 aerosol (R^2=0.90) (Fig. 1D). The high correlation between the product of O_3 abundance and
149 surface area density and $P(Cl_2)$ is not necessarily the result of a causal relationship between O_3
150 and Cl_2, but likely highlights their photochemical co-production. In other words, we suggest
151 that this is a consequence of the chemistry rather than the cause of the Cl_2 production.

152   Instead, these observations suggest that photochemistry on the particle surfaces is the
153 important driver of the high Cl_2. The strong correlation between $P(Cl_2)$ and the product of
154 nitrate and aerosol surface area density suggests that photolysis of nitrate-laden particles may
155 be involved in the chloride activation to produce Cl_2 at our site. The Cl_2 production via chloride
156 activation also requires particulate chloride. Interestingly, the average chloride (Cl^-)
157 concentrations were comparable in the oceanic air with low Cl_2 (0.56 μg/m^3 in $PM_{2.5}$ and 2.47
158 μg/m^3 in PM_{10}) and the continental air mass (0.50 μg/m^3 in $PM_{2.5}$, 2.38 μg/m^3 in PM_{10}). The
159 average Cl/Na mass ratio in the oceanic air was 1.48 in $PM_{2.5}$ and 1.63 in PM_{10} compared to
160 1.10 in $PM_{2.5}$ and 1.33 in PM_{10} in continental air, indicating that Cl was less abundant in
161 polluted air than in the clean air, in comparison to their average ratio of 1.8 in seawater [29].
162 These results suggest that Cl^- was not the limiting factor, and the Cl_2 production was mainly
163 controlled by nitrate availability and other factors.

164
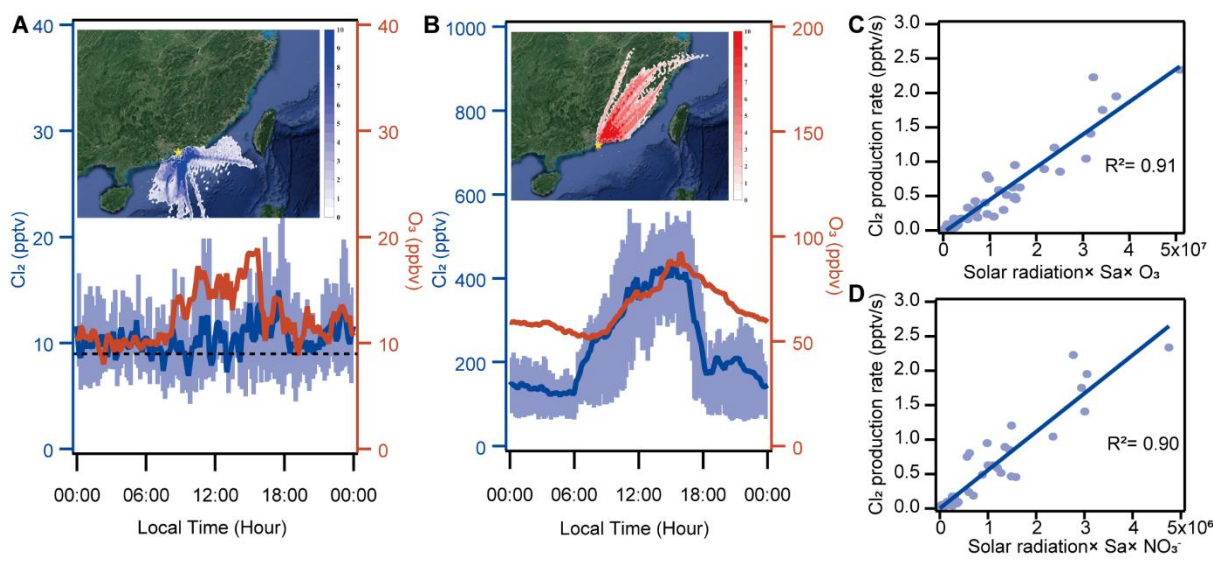
165

166 **Fig. 1. Ambient observations at Hok Tsui, Hong Kong, from 31 August to 9 October 2018.**
167 The diurnal profiles of Cl_2 and O_3 (**A**) in the air mass from the South China Sea (31 August - 4
168 September). The dashed line represents the detection limit of the CIMS instrument; (**B**) in the
169 air mass from the continental region (5 September - 9 October). The blue line is the 10-min
170 average of Cl_2, and the blue shade represents the 25 percentile and 75 percentile values. The

171 red line is the 10-min average of O_3. The inserts in (A) and (B) show the back trajectory of the
172 oceanic and continental air mass, respectively, during the measurement period. (**C**) The scatter
173 plot of the production rate of Cl_2 (P_{Cl2}) and the product of the solar actinic flux (W/m^2), the
174 aerosol surface area density (um^2/cm^3), and O_3 mixing ratio (ppb) from 08:00 to 18:00 in the
175 continental air mass. (**D**) The scatter plot of the production rate of Cl_2 (P_{Cl2}) and the product of
176 the solar actinic flux, the aerosol surface area density, and nitrate concentration in PM_{10} (ug/m^3)
177 from 08:00 to 18:00 in the continental air mass. The P_{Cl2} equals the photolysis rate of Cl_2 (J_{Cl2}
178 × measured Cl_2 concentration) as Cl_2 was near a photo stationary state. J_{Cl2} was calculated from
179 the TUV model (http://cprm.acom.ucar.edu/Models/TUV/Interactive_TUV) under clear sky
180 conditions and then scaled to the solar radiation derived J_{NO2} (see Methods section 3).

181

**Laboratory investigations of Cl_2 production**

183   To explore the photochemistry leading to Cl_2 production, a series of experiments were
184 undertaken by illuminating nitrate and chloride-containing solutions and ambient aerosols in
185 the presence of gaseous O_3 with a high-pressure xenon lamp (Fig. S6). The experimental setup
186 and detailed information (designs, lamp, and chemicals) are given in Methods section 5 (and
187 Fig. S7). The average relative humidity (RH) during the field measurements was 81%, which
188 was above the deliquescence point of NaCl (75%), and thus a very large fraction of sea-salt
189 aerosols should have been wet during our field study. We, therefore, investigated Cl_2
190 production over or in solutions.

191   No Cl_2 was observed in the blank experiments, which were run with an empty chamber
192 or with a quartz petri dish containing deionized water or chloride placed in the chamber, in the
193 dark or when illuminated by the xenon lamp. We also did not detect Cl_2 when the zero air
194 containing various O_3 mixing ratios (150, 250, and 500 ppbv) flowed over the illuminated
195 chloride solution (1 M) with the pH ranging from 3.3 to 6.8. One example is shown in Fig. S8.
196 The result shows that O_3 photolysis alone does not produce any detectable amount of Cl_2 in our
197 experiment, as observed previously [26]. We note that the rate constant for O_3 to generate $O(^1D)$
198 (1.31×10^{-5} s^{-1}) in our experiment was two orders of magnitude lower than that in previous study
199 [26], which used a more intense UV light source.

200   Interestingly, we observed significant Cl_2 production when acidic solutions (pH <3.3)
201 containing both chloride and nitrate were illuminated. Irradiation of the solution, with an initial
202 pH of 1.9, led to a continuous increase of gaseous Cl_2, and up to 3.5 ppbv was observed after
203 500 minutes of illumination (Fig. 2A). There was no increase in the Cl_2 signals when the zero
204 air containing differing O_3 mixing ratios (150, 250, and 500 ppbv) flowed over the illuminated
205 chloride-nitrate solutions with a pH of 1.9 to 2.9. One example is shown in Fig. S8. When we
206 placed an AM1.5 optical filter in front of the xenon lamp, which only allows the light with the
207 wavelength > 360nm to pass through, there were a sharp decrease in the Cl_2 (and HONO)
208 signals (shown at t = 540 min), whereas using a 300-800nm optical filter (allowing the 300-
209 800nm light to pass through) only slightly decreased the Cl_2 (and HONO) production (shown

at t=520 min). This result reveals large Cl_2 production occurring at the wavelength of <360 nm despite its concurrent significant photolytic loss.

Based on the above results, we propose that the hydroxyl radical (OH) from the nitrate photolysis and subsequent oxidation of chloride in solution was primarily responsible for the observed high rate of Cl_2 production (R12-R14, R4, R5).

$$NO_3^- + hv \text{ (<350 nm)} \rightarrow O^- + NO_2 \text{ (aq)} \text{ (R1, yield~0.01)} \quad \text{(R12)}$$

$$\rightarrow NO_2^- + O(^3P) \text{ (aq)} \text{ (R2, yield~0.001)} \quad \text{(R13)}$$

$$O^- + H^+ \rightarrow OH \text{ (aq)} \quad \text{(R14)}$$
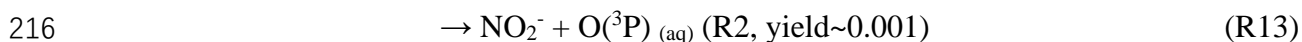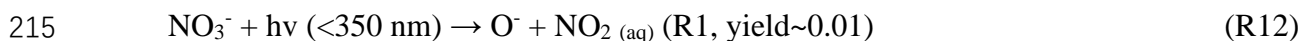
It has been known that nitrate absorbs light in the actinic range of 290-350nm and dissociates via two pathways (R12 and R13) with a quantum yield of 0.01 and 0.001, respectively [30-33]. O^- (produced from R12) reacts with water to form the hydroxyl radical (OH) (R14). This process can be accelerated by the acidity of the solution [30]. The produced OH can further oxidize Cl^- to produce Cl_2 in the liquid phase (R4-R5), according to previously known aqueous chemistry [26,34], and a portion of the Cl_2 is released to the gas phase. Our observation of HONO and NO_2 production (see Fig. 2A, 2B) supports that R12 and R13 were taking place in our experiment and is consistent with the previous studies showing the production of HONO and NO_2 from illuminated nitrate solutions [35]. To confirm the role of aqueous OH radical in the Cl_2 production, we added 10µl 0.1M Tert-Butyl Alcohol [36] (TBA, an OH radical scavenger with a rate constant of $3.8-7.6 \times 10^8$ M^{-1} s^{-1}) in the lit solution (Fig. 2B). There was a sharp decrease of the Cl_2 signal lasting for 20 minutes before returning to the previous level. To make sure that this change was not caused by operation (i.e., opening the chamber), we added 10ul DI water into the chamber, and the Cl_2 signal bounced back in a few seconds. This result confirmed that the aqueous OH radical played a significant role in the Cl_2 production in the chamber.

We found that the Cl_2 production was strongly dependent on the acidity of the solution (Fig. 2C and Fig. S9). The production rate sharply dropped to near zero when the pH increased from 2.9 to 3.3. It is expected that increasing pH would decrease the OH radical production via R14 and decrease the reaction rate of the Cl_2 output via R5 [27]. In addition, when the pH increases (H^+ decreasing), nitrite ions (NO_2^-) would produce less HONO in the aqueous phase, which in turn produces less aqueous OH radical (via R15) and then Cl_2. Interestingly, there seems a critical pH (~3.3) above which little Cl_2 is produced. This can be explained by suppression of OH by NO_2^- above this pH value of 3.3. The dissociation constant (pKa) of HONO at 298K is 3.3 [37,38], i.e., above pH=3.3, NO_2^- is the predominant species in solution. We found that NO_2^- can efficiently suppress OH concentration. When we added a very small amount of NO_2^- (10ul 0.01M) in the lit solution, the concentration of Cl_2 decreased significantly (Fig. 2B), revealing that NO_2^- is an OH scavenger. Figure 2B shows that it took twice as long for the Cl_2 signal to return to the previous level, compared to the case of TBA, suggesting that NO_2^- is a more efficient OH scavenger than TBA. In summary, based on our experimental results, we hypothesize that the photolysis of nitrate has two different effects on Cl_2 production. One is to promote Cl_2 production by increasing OH (R4-R5), and the other is to inhibit Cl_2

250 formation via nitrite. Increasing solution pH allows more NO_2^- to stay in the solution and
251 reduces Cl_2 production.

252 $$NO_2^- + H^+ \rightleftharpoons HONO \ (aq) \rightarrow HONO \ (g) \qquad\qquad (R15)$$
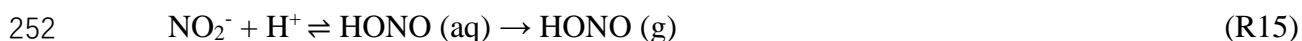
253 To further investigate the daytime Cl_2 formation under ambient conditions, four aerosols
254 samples collected (for 24-hour duration each) at the same site on 11-13 October 2020 were
255 irradiated in the dynamic chamber. As shown in Fig. 3A and Table. S2, Cl_2 mixing ratios of up
256 to 600 ppt were observed after illumination two of the aerosol particle-loaded filters (filter 01
257 and 02) containing high concentrations of Cl^- and NO_3^-. Interestingly, the produced Cl_2 were
258 below the detection limit in the other two filters (filter 03 and 04) loaded with particles that
259 contain low concentrations of Cl^- and NO_3^-. In filter 01, the high level of Cl_2 was observed
260 along with HONO, suggesting the potential role of particulate nitrate photolysis in their
261 productions. Similar to the experiment performed on the Cl^- and NO_3^- solution, the Cl_2 levels
262 decreased with the use of AM1.5 optical filter, indicating the wavelengths <360nm were very
263 important for Cl_2 (and HONO) production, and no increase in Cl_2 was observed when we
264 flowed the zero air containing 250 ppbv O_3 (Fig. 3A). These results suggest that photolysis of
265 particulate nitrate could produce a considerable amount of Cl_2 in the daytime. The photolysis
266 of nitrate induces an "OH burst" localized on/in an aerosol particle that activates Cl radicals
267 leading to the production of Cl_2 in the condensed phase. This Cl_2 produced in the condensed
268 phase outgases into the gas phase and impacts the gaseous oxidation capacity (see below). This
269 is an interesting coupling between condensed phase oxidation capacity and its gaseous
270 counterpart. The presence of condensed particles allows for the accumulation of high
271 concentrations of chemicals in them and enables this phenomenon. Interestingly, "OH burst"
272 has also been recently recognized under different conditions than those reported here, i.e.,
273 during the formation of cloud droplets [39] and are therefore potentially ubiquitous. The Cl
274 activation and subsequent Cl_2 production would occur on aerosols where high concentrations
275 of OH are produced, in the current case by the nitrate photolysis, in the presence of chloride
276 anions.

277 We next attempt to extrapolate the laboratory results to account for the observed
278 atmospheric daytime Cl_2. The field observations suggest that the Cl_2 production likely occurs
279 on the aerosol surface. Our experiments on liquid solution indeed showed increasing Cl_2
280 production rates with available surface areas of the solution (Fig. S9). The pH for most aerosol
281 samples (>90%) in the 2018 field campaign was in the range of 1-3, with an average value of
282 1.5 (Fig. S10), which was estimated from the E-AIM model (see Methods section 2). The
283 laboratory-determined Cl_2 production rates on liquid solutions at pH of 2.0~3.0 (similar to that
284 of ambient aerosol) and 1mol/L nitrate were 22-114 pptv/s (shown at t = 520min in Fig. 2).
285 The surface area density of the solution in the chamber air is 5.13×10^5 um^2/cm^3 (see Methods
286 section 5), which gives a Cl_2 production rate of 43 to 214 mol/m^2. For the continental air mass
287 and during the period of 10:00-15:00, the average surface area density of ambient aerosols was
288 653 um^2/cm^3 after taking into account aerosol hygroscopicity when assuming the particles to
289 be spherical, and the nitrate concentration in the aerosol liquid phase estimated by the E-AIM
290 model was 3.9 mol/L. This gives an estimated Cl_2 production of 0.11-0.57 pptv/s, which could
291 explain 13-68% of the observed average Cl_2 production rate (~0.84 ppt/s) in the ambient air.

292 In addition to the airborne aerosol, the Cl_2 production may occur on the aerosols deposited on
293 the ground, which could provide additional production that would help to reconcile the lab and
294 field observed Cl_2 productions.

295   Our study demonstrates that Cl_2 can be produced from photolysis of aerosol containing
296 nitrate, chloride, and high acidity. Such a production mechanism may occur in many parts of
297 the world impacted by anthropogenic pollution. Despite a significant reduction in the emissions
298 of acid precursors like sulfur dioxide (SO_2) and nitrogen oxides (NO_x), highly acidic aerosols
299 are still present in some areas/seasons in Asia, North America, and Europe [40], and nitrate
300 aerosols are also abundant in world's urban and industrial regions [41,42]. Previous studies have
301 also indicated the ubiquity of aerosol chloride in continental as well as maritime environments
302 [3,29,43]. We, therefore, anticipate that the Cl_2 production operates in many places or times
303 where/when sufficiently high levels of acidity, nitrate, and chloride co-exist. We also note that
304 elevated nitrate and the other acidic aerosol (sulfate) have been observed during the Arctic haze
305 events [44,45] and suggested in the Antarctic's stratospheric clouds [46,47]. It would be of great
306 interest to investigate whether the nitrate photolysis mechanism would contribute to the
307 liberation of inert chlorine in the polar atmosphere, in addition to the widely accepted
308 heterogeneous production of Cl_2 of HOCl and $ClONO_2$ with HCl (i.e., R10 and R11).

309
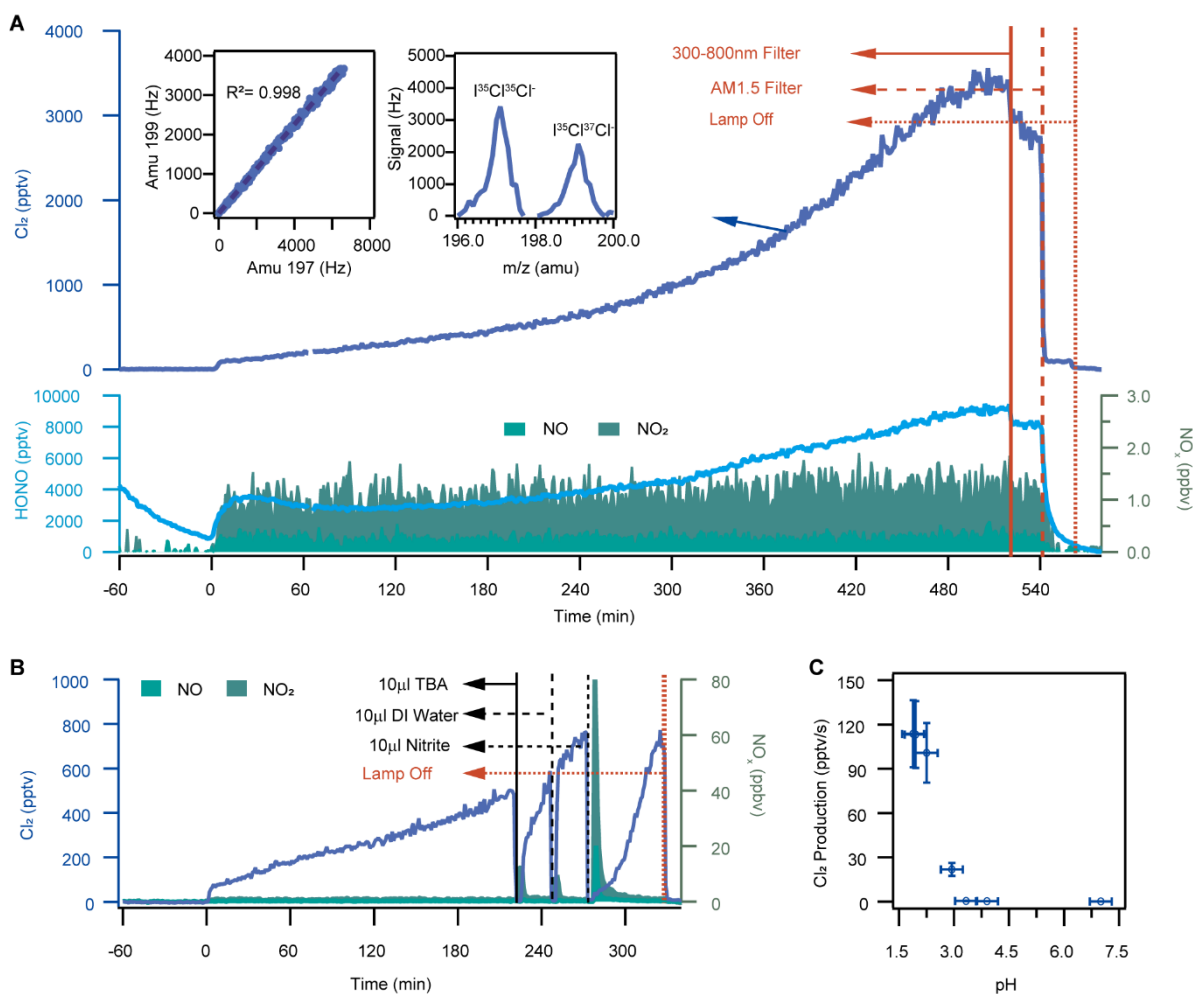
Fig. 2. Experimental results on solutions in the dynamic chamber. (**A**) Time series of 1-min average mixing ratios of Cl_2, HONO, and NO_x. The liquid solution samples (pH=1.9) were illuminated at t=0. The solid red line shows the time at which 300-800 nm filter was used, the red dashed line indicates the time at which AM1.5 filter was used, and the red point line indicates the time at which the xenon lamp was turned off. The left inset: scatter plot of the raw CIMS signal of Cl_2 at mass 199 atomic mass unit (amu) ($I^{35}Cl^{37}Cl^-$; $I^{37}Cl^{35}Cl^-$)) versus 197 amu ($I^{35}Cl^{35}Cl^-$) with 1-min average from t=-60 to t=580min. The right inset: the scanned mass spectra from 196 amu to 200 amu at t = 387min. The continuous increase of Cl_2 may be due to the higher concentration of ions and acidity in the solution due to the evaporation of water from the solution. (**B**) Time series of 1-min average Cl_2, NO, and NO_2. The liquid solution samples (pH=2.0) were illuminated at t=0. The solid black line shows the time at which 10ul OH scavenger, TBA, was added, the black dashed line indicates the time at which 10ul DI water was added, the black point line indicates the time at which 10ul nitrite was added, and the red point line indicates the time at which the xenon lamp was turned off. (**C**) The production rate of Cl_2 as a function of initial solution pH (pH= 1.9;2.0;2.3;2.9;3.3;3.9;6.8) at the illumination time of 500min. The error bars in plot (C) represent the estimated uncertainty in Cl_2 and pH measurement. Experimental conditions: 75−83% RH, 298 K in air and one 4 ml liquid solution containing 1M NaCl + 1M $NaNO_3$.

Impact on atmospheric chemistry and implications

We assess the effects of the observed Cl_2 on VOC oxidation using a photochemical box model with up-to-date VOC-Cl chemistry [6] (also see Methods section 3) by constraining the model with the measured Cl_2 abundance and other relevant observations for 4 -14 September 2018. The average values and the diurnal profiles of the input data indicate moderately polluted conditions for this period, with an average peak mixing ratio of O_3 of ~80 ppb and Cl_2 of 300 ppt and NO_x and VOCs levels characteristic of the polluted rural environment (Supplementary Table. S1, and Fig. S4). The model predicted that Cl atoms reached a maximum concentration of ~2.5×10^5 cm^{-3} at noon (Fig. S11A), with Cl_2 photolysis being the dominant source (~85%) (Fig. 3B). The peak Cl production rate at our site (~4×10^7 $cm^{-3}s^{-1}$, Fig. 3B) is more than five to six times of that from the photolysis of BrCl and Cl_2 in winter [6] or from the photolysis of Cl_2 (predominantly) and $ClNO_2$ in summer in a rural area of northern China [18], and is two orders of magnitude larger than that from the photolysis of Cl_2 and $ClNO_2$ in late autumn and early winter at a ground site near the City of Manchester, UK [19].

The Cl atoms accounted for 59% of daily integrated oxidation of non-methane alkanes, 16% of aromatics, 13% of aldehydes, and 9% of dialkenes (Fig. S12). The reactions of Cl atoms with VOCs produce RO_2 radicals, which are recycled to form HO_2 and OH radicals, thereby collectively increasing the average mixing ratios of OH, HO_2, RO_2 radicals by ~4%, ~17%, and ~27%, respectively (Fig. S11). The enhanced HO_2 and RO_2 by Cl-VOC reaction increased the in-situ net total ozone (O_x, O_3+NO_2) production rates by 17% (or 1.6 ppb/h) and its daily integrated production by 16% (or 38 ppb/day) (Fig. S11), despite destroying ozone by Cl atoms at the same time (Fig. 3B). With a high-resolution time of flight mass spectrometer (HR-ToF-CIMS), we also observed elevated concentrations of organochlorides (e.g., 1-chloro-3-methyl-3-butanone, CMBO) with a similar diurnal profile to Cl_2, a possible indication of significant oxidation of VOCs by chlorine atoms (Fig. S13). These results demonstrate the substantial impact of Cl_2 on daytime oxidation chemistry at our moderately polluted site.

In summary, a limited number of prior studies have indicated the presence and important role of daytime Cl_2 in the photochemistry of the lower troposphere in polluted regions. However, the exact source or production mechanism remained uncertain, which has hindered the reproduction of the daytime Cl_2 in current state-of-the-art global and regional chemistry transport models. Our field and laboratory results reveal that photolysis of nitrate in the acidic chloride laden aerosol can be a large Cl_2 source in the daytime. The co-existence of ubiquitous anthropogenic and natural chloride sources and nitrate-containing acidic aerosol in many parts of the polluted troposphere implies the broad presence of this Cl daytime source. Our recent study in northern China also shows that nitrate photolysis could activate chloride and bromide in coal-burning aerosol, which exerted a large impact on winter oxidation chemistry [6]. These findings have indicated a previously unrecognized role of the reactive nitrogen cycle in reactive halogen and HO_x chemistry, which have important implications on atmospheric oxidation and production of secondary air pollutants. We call for more investigations of the roles of halogen chemistry in the polluted troposphere and suggest some research that would place Cl_2 (and other halogens) production and atmospheric impact on a firmer footing. They include detailed laboratory measurements of the photolysis of nitrate ion in aerosol as a function of acidity,

complete characterization of the aerosol particles to identify the origin of chloride in them, robust ways to determine rates of photolysis in and on aerosol particles, and parameterization of Cl_2 production to assess the broader impact of reactive chlorine chemistry in regional and global models.
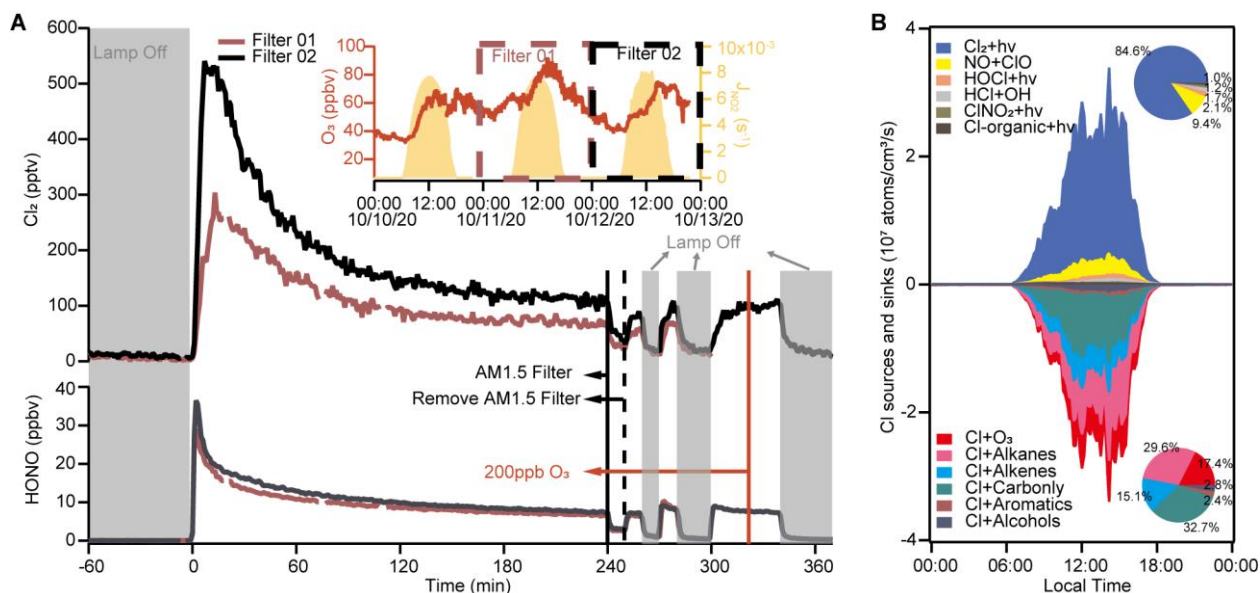

Fig. 3. (A) Experimental results on ambient aerosols in the dynamic chamber. Time series of 1-min average Cl_2 and HONO. Ambient samples (cropped size: 60mm × 60mm, Fig. S7C) were illuminated at t=0. The grey area indicates the period which the xenon lamp was turned off, the solid black line shows the time at which the AM1.5 filter was used, the black dashed line indicates the time at which the AM1.5 filter was removed, and the solid red line indicates the time at which 250 ppbv O_3 was added. The right inset: ambient observations of O_3 and J_{NO2} during the ambient aerosol collection in October 2020. Experimental conditions: 75−83% RH and 298 K in air. **(B)** The model-calculated average diurnal profiles of sources and sinks of the Cl atom for period 4 -14 September 2018. Upper right inset: the daytime average contribution from different sources to Cl atom. Bottom right inset: the average daytime contribution from different sinks to Cl atom.

Author contributions: T.W. and X.P. designed the Cl_2 research. T.W. and C.G. coordinated the field observations. X.P. designed the laboratory experiments with significant contribution from W.W., A.R.R., C.G., T.W. and Y.M.. X.P., W.W., and M.X. performed halogen measurements. W.W., Y.W., and X.W. performed HONO measurements. W.W. and M.X. performed solar radiation field measurements. C.Y. performed aerosol size distribution measurement. M.C., A.M., Y.M., M.S., C.L., K.L., and A.Y. provided VOCs measurement data. M.C., A.M., Y.M., SC.L., performed OVOCs measurement. C.M.S., and M.H. performed the organochlorides measurement with HR-Tof-CIMS. X.L., and H.G. collected ambient filters and performed ionic composition analysis. X.P. performed the laboratory work with the help from W.W., M.X., C.Y., C.P., Q. L., and Y.W. W.W. and X.P. conducted the chemical box model simulation. M.X. ran the E-AIM model for the calculation of the molar concentrations of inorganic ions. J.D. conducted the back-trajectory simulation. X.P., T.W., W.W., A.R.R., and C.G. analyzed the field, laboratory, and modeling results with significant contribution from Q.L., A.M., Y.M., M.H., A.S-L., H.H., and J.C. T.W. and X.P. wrote the paper with significant input from A.R.R., C.G., and A.S-L. All authors reviewed and commented on the final paper.

Competing interests: The authors declare that they have no conflict of interest.

Data and materials availability: Field measurement and lab study data are available by contacting the corresponding author (T.W.) (cetwang@polyu.edu.hk).

Methods

Section 1, Field measurements

Cl_2, $ClNO_2$, HONO, NO, NO_2, O_3, volatile organic compounds (VOCs), oxygenated volatile organic compounds (OVOCs), aerosol compositions (including/e.g., Na^+, NH_4^+, SO_4^{2-}, NO_3^-, Cl^-), solar radiations, and other meteorological parameters were measured from 31 August to 09 October of 2018 at the Hong Kong Environmental Protection Department's Cape D'Aguilar Super Site which is situated at the southeast corner of Hong Kong Island (Fig. S1). We introduce in detail Cl_2 and other species measured by a chemical ionization mass spectrometer (CIMS). Information on other measurements is summarized in Table. S3.

Reactive chlorine species (including Cl_2, $ClNO_2$, and HOCl) and HONO were measured by a quadrupole CIMS (Q-CIMS). A detailed description of the CIMS and ion chemistry has been described in our previous studies [6,16]. Briefly, Iodide (I^-) was used as a reagent ion. Cl_2 was monitored at 197 amu ($I^{35}Cl^{35}Cl^-$) and 199 amu ($I^{35}Cl^{37}Cl^-$), $ClNO_2$ at 208 amu ($I^{35}ClNO_2^-$) and 210 amu ($I^{37}ClNO_2^-$), HOCl at 179 amu ($IHO^{35}Cl^-$) and 181 amu ($IHO^{37}Cl^-$), and HONO at 174 amu. In this study, we used the data of Cl_2, $ClNO_2$, and HONO from CIMS measurement. The HOCl signals suffered from spectral interference, as indicated by the weak correlation between the two isotopic masses, and thus were not used in further analysis.

The instruments were housed in a one-story building. The inlet is a 3.5-m long PFA-Teflon tubing (1/2 in. outer diameter) with 1.5 m of it situated above the roof. We adopted the previous inlet design as described in our previous study [6]. To further reduce the residence time (and thereby potential artifacts) in the inlet tubing, we used a blower with a flow rate of 500 LPM flow to draw the sample. As a result, the residence time of the sample air in the inlet tubing was below 0.1 s. To reduce the particle deposited on the inlet tubing, the tubing was flushed with DI water and then dried by drawing ambient air for 20 minutes every three days.

The following on-site and post-measurement measures were undertaken to ensure accurate measurements of Cl_2. They included **(1) Instrument background determination.** During the study, the CIMS background signals were determined about every two days by scrubbing ambient air with alkaline glass wool and charcoal [6]. Many inorganic halogens are efficiently removed by this process. In the present study, the background for Cl_2 was small and relatively stable at around 5 pptv during the field campaign (Fig. S14B). The 2-σ detection limit was 9 pptv for Cl_2 (at 197 amu). **(2) Regular calibration with a Cl_2 standard.** The calibration of Cl_2 was conducted on-site every 2-4 days with a Cl_2 permeation tube. The detailed calibration methods have been described in our previous study [6]. The permeation rate of the Cl_2 standard was determined before and after the campaign and was stable at around 210 ng/min, with a variation of less than 5% during the field campaign. The sensitivity of Cl_2 was stable at 2.0 Hz/pptv with a standard deviation of 0.2 Hz/pptv, as shown in Fig. S14D. The Cl_2 sensitivity was invariant at RH of 20-80% (Fig. S14E). The measurement uncertainty for Cl_2, calculated from the variation of the sensitivity during the

14

455   campaign and the uncertainty of permeation tube source, was about 11%. **(3) Examination of the**
456   **isotopic ratio of the detected compounds.** During the field study, we confirmed that the detected
457   signal for Cl_2 had no significant spectral interference. The two isotopic masses at 197 amu and 199
458   amu were well resolved, as shown in Fig. S14A, and showed excellent correlation (R^2=0.93) with
459   a slope of 0.63 (Fig. S14C), which is similar to the theoretical value of 0.65. **(4) Investigation of**
460   **conversion on inlet surfaces.** We conducted a series of tests to examine potential inlet
461   interferences in the field and laboratory, which included: (i) potential inlet artifact tests of O_3 and
462   N_2O_5 heterogeneous reactions on-site by scrubbing the ambient air. Cl_2 often coincided with high
463   O_3 concentrations in the field, and the previous lab [48] and field studies [16] indicate potential Cl_2
464   formation involving N_2O_5. During the field sampling period, when we turned off the bypass blower
465   and injected concentrated O_3 and N_2O_5 into the ambient air sample (resulting in 250 ppb of O_3 and
466   5 ppbv of N_2O_5 after mixing with the ambient air), we did not observe any increased Cl_2 signals.
467   This result indicates that the O_3 and N_2O_5 did not produce detectable artifacts in our Cl_2
468   measurement. (ii), potential inlet artifact tests of HOCl reactions in the laboratory. A previous
469   study reported that 15% of the HOCl was lost in their NaCl-coated inlet, with 2% converting to
470   Cl_2 [11]. Our post-campaign tests confirmed that the observed Cl_2 did not suffer from significant
471   interference from HOCl in the sampling inlet. Briefly, we tested two types of Teflon tubing: one
472   used in the campaign and a new tubing with the same length. HOCl was synthesized using a
473   phosphate-buffered solution (pH = 6.8) of NaOCl (11-14% chlorine, Alfa Aesar) and $AgNO_3$,
474   analogous to the previous method [11,13]. A 20 sccm dry N_2 was flowed through the solution and
475   then diluted into 6 SLPM humidified zero air. The concentration of HOCl was calculated from the
476   Cl_2 formation by passing the HOCl standard through a NaCl-coated tubing. For the HOCl inlet
477   conversion test, the synthesized HOCl mixed with 6 SLPM humidified zero air was first introduced
478   to the CIMS without passing through the tubing. Then, the HOCl/air mixture passed through the
479   tubing before entering the CIMS. The decrease in the HOCl signal and the increase in the Cl_2
480   signal induced by the tubing were monitored to determine the conversion of HOCl to Cl_2 in the
481   tubing. Under the RH condition similar to the field campaign, we found that 31% and 7% of the
482   HOCl were lost, and 18% and 2% were converted to Cl_2 in the used tubing and the new tubing,
483   respectively. As the flow rate in the laboratory (6 SLPM) was much lower than the ambient sample
484   flow rate (500 SLPM), we conclude that the conversion rate of HOCl to Cl_2 during the field
485   measurement should be much lower than 18%.

486

487   **Section 2, HYSPLIT and E-AIM models**

488   Three-day (72 hours) backward trajectories were calculated for each hour using the Hybrid

489   Single - Particle Lagrangian Integrated Trajectory (HYSPLIT) model

490   (https://www.ready.noaa.gov/HYSPLIT.php). The HYSPLIT was driven by 3-hourly archive data

491 from NCEP's GDAS with a spatial resolution of 1 degree by 1 degree. The endpoint of the
492 trajectories was 300 m above ground level at Hok Tsui, which is in the middle of the marine
493 boundary layer. Air masses were then classified based on the source regions (ocean or continent).

494 The H^+ concentrations ($[H^+]$, in mol/L) in the aqueous phase of aerosols were calculated
495 using the E-AIM model (E-AIM III) online
496 (http://www.aim.env.uea.ac.uk/aim/model3/model3a.php) [16,49]. The inputs to the model are hourly
497 measurements of ambient RH and molar concentrations (unit: mol/m^3) of Cl^-, NO_3^-, SO_4^{2-}, Na^+,
498 and NH_4^+ in $PM_{2.5}$, which were measured by an ion chromatography (MARGA, see SI) and gas-
499 phase ammonia. Aerosol pH was estimated as the negative logarithm of $[H^+]$ without further
500 consideration of the activity coefficient of ions in the aqueous phase.

501

502 **Section 3, Chemical box model**

503 A zero-dimensional gas-phase chemical box model was used to calculate the budget for Cl
504 atoms and to evaluate the observed Cl_2 on atmospheric oxidation. The detailed information on the
505 mechanisms and their related kinetics data of gas-phase reactions adopted in the model is given in
506 the previous study [6]. The measured values of Cl_2, $ClNO_2$, N_2O_5, HONO, O_3, NO, NO_2, SO_2, CO,
507 and temperature were averaged or interpolated every minute and constrained into the model. The
508 measured VOCs and OVOCs (except for CH_4 and HCHO) were interpolated every minute and
509 constrained into the model. The mixing ratio of CH_4 was kept at a constant value of 2000 ppbv [50].
510 As the HCHO measurement data was not available in the 2018 field campaign, we used the HCHO
511 measurement data obtained during September 2020 by off-line DNPH-Cartridge-HPLC (24h-
512 average, 3.3 ppb) and adjusted for its diurnal variation according to a typical HCHO profile in a
513 non-urban environment [51]. The input data for HCHO is shown in Fig. S4.

514 The photolysis frequencies for Cl_2, HONO, O_3, and other species were calculated from the
515 TUV model (http://cprm.acom.ucar.edu/Models/TUV/Interactive_TUV/) under clear sky
516 condition and then scaled to J_{NO2}, which was derived from the measured solar radiation and
517 relationship with J_{NO2} for Guangzhou (~100km north of the present site) [52]. The dry deposition
518 process in the model was represented by a first-order loss reaction, using the same parameter
519 described in the previous study [53]. The boundary layer height was set at 200 m at nighttime and
520 1500 m for daytime in the model. The wet deposition was ignored as no rainfall event occurred
521 during the observation period. The model was run from 00:00 of 4 September to 00:00 of 14
522 September, and the simulation for the first 24 h was repeated three times to stabilize the
523 intermediate species. A summary of the input parameters in the model is shown in Table. S1, and
524 the diurnal patterns of select input data are shown in Fig. S4.

525

526

Section 4, Estimation of Cl₂ production from heterogeneous reactions of HOCl

Cl₂ can be produced from heterogeneous reactions of gaseous HOCl on a chloride-containing solution, with an uptake coefficient of HOCl up to 0.0002 [21,54]. We used the following equation (Eq.1) to estimate the Cl₂ production rate from the HOCl heterogeneous reaction.

$$\text{The Cl}_2 \text{ production rate } = \frac{d[\text{HOCl}]}{dt} = \frac{1}{4}c_{HOCl}\gamma S_a[HOCl] \quad \text{(Eq.1)}$$

Where c is the mean molecular speed of HOCl, γ is the heterogeneous uptake coefficient of HOCl, [HOCl] is the model simulated concentration, and S_a is the aerosol surface area density.

Section 5, Lab experiments

5.1. The laboratory design

A dynamic reaction chamber was used to measure the productions of Cl₂ by illuminating nitrate-NaCl solution and aerosol collected on filters. The overall experimental setup is shown in Fig. S7 and is described here. The chamber is made of TFE Teflon (1.875L, 25cm-length × 15cm-width × 4cm-height) with a TFE Teflon-film window on the top. A quartz petri dish (inner diameter: 35mm, internal height: 7mm) held 4-ml liquid solution or filter samples. The surface area density of the chamber was determined as the physical surface area of the solution in the petri dish divided by the chamber's volume and was 513,127 um²/cm³. Zero air (2.9 LPM) with adjustable humidity (75-83%) flowed through the chamber. The experiments were conducted at room temperature (296 K). A flow of O₃ was diluted by zero air and then added into the chamber with the resulting O₃ mixing ratio in the chamber ranged from 0 to 500 ppb. The residence time of the zero air/O₃ was 0.625 minutes in the chamber. The outflow of zero air carrying the reaction products was monitored in real-time by the same iodide-CIMS instrument used in the field for Cl₂ (amu 197, 199) and HONO (amu 174) detection and by a chemiluminescent/photolytic converter for NO and NO₂.

To mimic the spectrum of the solar radiation, a high-pressure xenon lamp was used as the light source, and its spectral irradiance is shown in Fig. S6. It covers from 320nm to 1100nm and peaks at 450nm. Compared to the solar irradiance at a solar zenith angle of 48.2° (i.e., an air mass factor of 1.5 and standard ozone column abundance), the xenon lamp has a smaller flux in the range of 300 nm - 326 nm but a larger flux in the range of 326 nm - 420 nm. The photolysis rate constant for O₃ to generate O^{1}D (1.31×10^{-5} s^{-1}) was similar to the daytime averaged rate constant of 1.78×10^{-5} s^{-1} (calculated from the TUV model under clear sky conditions) in the ambient air at our site (see following section 5.3), and the photolysis rate constant of Cl₂ (J_{Cl2}) in our chamber (5.80×10^{-3} s^{-1}, see below) was about four times larger than daytime averaged rate constant of 1.20×10^{-3} s^{-1} (calculated from the TUV model under clear sky conditions) in ambient air at our site. To investigate the role of photon energies, two optical filters were used (one is a 300-800nm filter,

562   which let the light with a wavelength of 300-800nm to pass through, and the other, AM1.5 filter,
563   which allows the light with the wavelength > 360nm to go through).

564   To investigate the potential production of Cl_2 in chloride and nitrate-containing solution,
565   sodium chloride (NaCl, ACS, >99.8%) and sodium nitrate ($NaNO_3$, Sigma-Aldrich, >99.0%) were
566   used as the source of particulate chloride and nitrate, respectively. Both NaCl and $NaNO_3$ were
567   prepared as 1M/L, which was similar to the average concentration of aqueous phase chloride and
568   nitrate in ambient aerosols in the field study, which was estimated from the E-AIM (see above).
569   The pH was adjusted by adding sulfuric acid (H_2SO_4, Sigma-Aldrich, 95%-97%) and measured
570   with a digital pH meter (HANNA instrument, HI253). In the experiments on the ambient filters,
571   the aerosols of $PM_{2.5}$ collected on quartz fiber filters with a high-volume sampler (Flow: about 890
572   L/min, sampling period: 23.5 h, size: A4 page) were placed in the chamber.

573

5.2. The CIMS measurements in the laboratory

575   As was done in the field study, we conducted instrumental background checks, isotope
576   analysis, and daily Cl_2 calibration in the laboratory experiments. The background for Cl_2 and
577   HONO was stable. The sensitivity of Cl_2 was stable at around 1.9 Hz/pptv with a standard deviation
578   of 0.1 Hz/pptv. HONO was calibrated at the end of the lab experiment. The sensitivities for HONO
579   during the laboratory studies were determined according to its sensitivity ratio relative to that for
580   Cl_2. The sensitivity for HONO was 3.0 Hz/pptv. The measurement uncertainty for Cl_2, calculated
581   from the propagation of relative standard deviation for one-minute average data and the variation
582   of the sensitivity within one day based on the calibration from permeation tube source, was about
583   5%. And measurement uncertainty for HONO, calculated from the propagation of both relative
584   standard deviation for one-minute average data and the variation of the sensitivity, was about 15%.

585

5.3. The determination of the photolysis rate and production rate of Cl_2.

587   The photolysis rate of Cl_2 (J_{Cl2}) in the chamber was calculated using the following equation
588   (Eq.2)

$$J = \int q(\lambda)\sigma(\lambda)I(\lambda)d\lambda \ (Eq.2)$$

590   Where q(λ) is the quantum yield at wavelength λ (nm), $\sigma(\lambda)$ is the cross-section of Cl_2 at

591   wavelength λ, which is adopted from the recommended value by IUPAC (http://iupac.pole-
592   ether.fr/index.html). I(λ) is the flux of xenon lamp at wavelength λ and was calculated by
593   converting the irradiation energy spectra of the lamp (Fig. S6) to photon flux based on Planck's
594   equation. The same method was used to calculate the photolysis rate constant for O_3 to generate

595   O^1D. The $q(\lambda)$ and $\sigma(\lambda)$ was adopted from the recommended value from IUPAC under 298 K

596   (http://iupac.pole-ether.fr/index.html).

597   All laboratory experiments were carried out under the same light intensity with the same

598   distance from the chamber (20cm). As shown in Fig. S7, almost the entire bottom area is

599   illuminated by light. Under this configuration, the J_{Cl2} was estimated to be 5.80×10^{-3} s^{-1} without

600   the optical filter, which was around four times larger than the daytime averaged photolysis rate

601   constant of 1.20×10^{-3} s^{-1} in the ambient air. In the calculation of J_{Cl2} in the chamber, we did not

602   consider light reflection at the Teflon window and in the chamber inner surface, as well as light

603   loss during transmission. The calculated J_{Cl2} was verified by another method, as shown at the end

604   of this section.

605   The production rate of Cl_2 (P_{Cl2}) in the dynamic chamber was determined based on the mass

606   balance. The P_{Cl2} is equal to the sum of the photolysis loss rate of Cl_2 and the advected loss of Cl_2

607   in the dynamic chamber using the following equation (Eq.3):

608   P_{Cl2} = photolysis rate of Cl_2 + advected loss of Cl_2 (Eq.3)

609   Thus, (Cl_2) $(pptv/s)$ = $[Cl_2] \times J_{Cl2} + [Cl_2] \times Q/V = [Cl_2] \times (5.8 \times 10^{-3}\ s^{-1} + 2.7 \times 10^{-2}\ s^{-1})$

610   under the experimental condition.

611   Where $[Cl_2]$ is the measured Cl_2 mixing ratio (pptv), J_{Cl2} is the calculated photolysis rate (s^{-1}), Q

612   is the flow rate of the zero air through the chamber (3 LPM), and V is the volume of the chamber

613   (1.875L). Equation (3) assumes negligible Cl_2 production from recombination of Cl atoms

614   produced from Cl_2 photolysis in the chamber, and this assumption is verified by the following

615   experiments: we compared the Cl_2 signals by the CIMS when 100 sccm a Cl_2 standard was diluted

616   by 2.9 SLPM zero air and further mixed with 100 sccm zero air or 100 sccm ozone-containing

617   zero air (yielding 500 ppbv ozone in the chamber air). These experiments were conducted without

618   the aerosol or liquid film in the chamber. There was no detectable change in the Cl_2 signals in the

619   two tests (i.e., with or without ozone). This result confirms little Cl_2 production from Cl back

620   reaction, as the Cl_2 signal with ozone added would have scavenged of Cl atom. Under the condition

621   of 3 SLPM flow (the condition of our experiments), advection was the predominant loss

622   (accounting for 82%) of Cl_2 produced in the chamber.

623   To verify the calculated J_{Cl2}, we compared the Cl_2 signals by the CIMS when the 100 sccm

624   Cl_2 standards diluted by 2.9 SLPM zero air (yielding 3.25 ppbv Cl_2 in the chamber air) and then

625   flowed through the chamber (without the condensed phase sample) with the lamp turned off and

626   then on. The experimental results showed that there was a 16.5% drop in the Cl_2 signals with the

627   lamp on. Using the above equation for P_{Cl2} (Eq.3), the J_{Cl2} was determined at 5.3×10^{-3} s^{-1}, which

628   is very close to the calculated value (5.80×10^{-3} s^{-1}) based on the lamp irradiance spectrum. Further,

629   the calculated extent of Cl atom recombination is roughly consistent with this assertion of a small

630   loss of Cl atoms due to recombination. Based on these experiments and calculations, we suggest

631   that the calculated J_{Cl2} is reliable.

632

References

1   Molina, M. J. & Rowland, F. S. Stratospheric sink for chlorofluoromethanes: chlorine atomc-atalysed destruction of ozone. *Nature* **249**, 810, doi:10.1038/249810a0 (1974).

2   Molina, L. & Molina, M. Production of chlorine oxide (Cl2O2) from the self-reaction of the chlorine oxide (ClO) radical. *Journal of Physical Chemistry* **91**, 433-436 (1987).

3   Thornton, J. A. *et al.* A large atomic chlorine source inferred from mid-continental reactive nitrogen chemistry. *Nature* **464**, 271, doi:10.1038/nature08905 (2010).

4   Wang, T. *et al.* Observations of nitryl chloride and modeling its source and effect on ozone in the planetary boundary layer of southern China. *Journal of Geophysical Research: Atmospheres* **121**, 2476-2489, doi:10.1002/2015JD024556 (2016).

5   Wang, D. S. & Ruiz, L. H. Secondary organic aerosol from chlorine-initiated oxidation of isoprene. *Atmospheric Chemistry and Physics* **17**, 13491-13508, doi:10.5194/acp-17-13491-2017 (2017).

6   Peng, X. *et al.* An unexpected large continental source of reactive bromine and chlorine with significant impact on wintertime air quality. *National Science Review*, doi:10.1093/nsr/nwaa304 (2020).

7   Li, Q. *et al.* Potential Effect of Halogens on Atmospheric Oxidation and Air Quality in China. *Journal of Geophysical Research: Atmospheres* **125**, doi:10.1029/2019JD032058 (2020).

8   Heimann, M. How Stable Is the Methane Cycle? *Science* **327**, 1211-1212, doi:10.2307/40544373 (2010).

9   Simpson, W. R., Brown, S. S., Saiz-Lopez, A., Thornton, J. A. & Glasow, R. V. Tropospheric halogen chemistry: sources, cycling, and impacts. *Chemical Reviews* **115**, 4035-4062, doi:10.1021/cr5006638 (2015).

10 Solomon, S., Garcia, R. R., Rowland, F. S. & Wuebbles, D. J. On the depletion of Antarctic ozone. *Nature* **321**, 755-758, doi:10.1038/321755a0 (1986).

11 Liao, J. *et al.* High levels of molecular chlorine in the Arctic atmosphere. *Nature Geoscience* **7**, 91, doi:10.1038/ngeo2046 (2014).

12 Spicer, C. W. *et al.* Unexpectedly high concentrations of molecular chlorine in coastal air. *Nature* **394**, 353-356, doi:10.1038/28584 (1998).

13 Lawler, M. J. *et al.* HOCl and Cl2 observations in marine air. *Atmospheric Chemistry and Physics* **11**, 7617-7628, doi:10.5194/acp-11-7617-2011 (2011).

14 Riedel, T. P. *et al.* Nitryl Chloride and Molecular Chlorine in the Coastal Marine Boundary Layer. *Environmental Science & Technology* **46**, 10463-10470, doi:10.1021/es204632r (2012).

15 Riedel, T. P. *et al.* Chlorine activation within urban or power plant plumes: Vertically resolved ClNO2 and Cl2 measurements from a tall tower in a polluted continental setting. *Journal of Geophysical Research: Atmospheres* **118**, 8702-8715, doi:10.1002/jgrd.50637 (2013).

16 Xia, M. *et al.* Significant production of ClNO2 and possible source of Cl2 from N2O5 uptake at a suburban site in eastern China. *Atmospheric Chemistry Physics* **20**, 6147-6158 (2020).

671   17   Impey, G. A., Shepson, P. B., Hastie, D. R., Barrie, L. A. & Anlauf, K. G. Measurements of
672   photolyzable chlorine and bromine during the Polar Sunrise Experiment 1995. *Journal of*
673   *Geophysical Research: Atmospheres* **102**, 16005-16010, doi:10.1029/97JD00851 (1997).
674   18   Liu, X. *et al.* High levels of daytime molecular chlorine and nitryl chloride at a rural site on the
675   North China Plain. *Environmental science & technology* **51**, 9588, doi:10.1021/acs.est.7b03039
676   (2017).
677   19   Priestley, M. *et al.* Observations of organic and inorganic chlorinated compounds and their
678   contribution to chlorine radical concentrations in an urban environment in northern Europe during
679   the wintertime. *Atmospheric Chemistry Physics* **18**, 13481-13493 (2018).
680   20   Le Breton, M. *et al.* Chlorine oxidation of VOCs at a semi-rural site in Beijing: significant
681   chlorine liberation from ClNO2 and subsequent gas- and particle-phase Cl–VOC production.
682   *Atmospheric Chemistry Physics* **18**, 13013-13030, doi:10.5194/acp-18-13013-2018 (2018).
683   21   Wang, X. *et al.* The role of chlorine in global tropospheric chemistry. *Atmospheric Chemistry and*
684   *Physics* **19**, 3981-4003, doi:10.5194/acp-19-3981-2019 (2019).
685   22   Wang, T., Lam, K. S., Lee, A. S., Pang, S. & Tsui, W. Meteorological and chemical
686   characteristics of the photochemical ozone episodes observed at Cape D'Aguilar in Hong Kong.
687   *Journal of applied Meteorology* **37**, 1167-1178 (1998).
688   23   Wang, T., Dai, J., Lam, K. S., Nan Poon, C. & Brasseur, G. P. Twenty-five years of lower
689   tropospheric ozone observations in tropical East Asia: The influence of emissions and weather
690   patterns. *Geophysical Research Letters* **46**, 11463-11470 (2019).
691   24   Dai, J. *et al.* The impact of sea-salt chloride on ozone through heterogeneous reaction with N2O5
692   in a coastal region of south China. *Atmospheric Environment* **236**, 117604 (2020).
693   25   Tham, Y. J. *et al.* Presence of high nitryl chloride in Asian coastal environment and its impact on
694   atmospheric photochemistry. *Chinese Science Bulletin* **59**, 356-359 (2014).
695   26   Oum, K. W., Lakin, M., DeHaan, D. O., Brauers, T. & Finlayson-Pitts, B. J. Formation of
696   molecular chlorine from the photolysis of ozone and aqueous sea-salt particles. *Science* **279**, 74-
697   76 (1998).
698   27   Knipping, E. *et al.* Experiments and simulations of ion-enhanced interfacial chemistry on aqueous
699   NaCl aerosols. *Science* **288**, 301-306 (2000).
700   28   Hoffmann, E. H., Tilgner, A., Wolke, R. & Herrmann, H. Enhanced Chlorine and Bromine Atom
701   Activation by Hydrolysis of Halogen Nitrates from Marine Aerosols at Polluted Coastal Areas.
702   *Environmental Science & Technology* **53**, 771-778, doi:10.1021/acs.est.8b05165 (2019).
703   29   Yang, X. *et al.* Abundance and origin of fine particulate chloride in continental China. *Science of*
704   *The Total Environment* **624**, 1041-1051, doi:10.1016/j.scitotenv.2017.12.205 (2018).
705   30   Mack, J. & Bolton, J. R. Photochemistry of nitrite and nitrate in aqueous solution: a review.
706   *Journal of Photochemistry Photobiology A: Chemistry* **128**, 1-13 (1999).
707   31   Benedict, K. B., McFall, A. S. & Anastasio, C. Quantum Yield of Nitrite from the Photolysis of
708   Aqueous Nitrate above 300 nm. *Environmental Science & Technology* **51**, 4387-4395,
709   doi:10.1021/acs.est.6b06370 (2017).

710 32 Scharko, N. K., Berke, A. E. & Raff, J. D. Release of Nitrous Acid and Nitrogen Dioxide from
711   Nitrate Photolysis in Acidic Aqueous Solutions. *Environmental Science & Technology* **48**, 11991-
712   12001, doi:10.1021/es503088x (2014).

713 33 Zellner, R., Exner, M. & Herrmann, H. Absolute OH quantum yields in the laser photolysis of
714   nitrate, nitrite and dissolved H2O2 at 308 and 351 nm in the temperature range 278–353 K.
715   *Journal of Atmospheric Chemistry* **10**, 411-425, doi:10.1007/BF00115783 (1990).

716 34 Abbatt, J. *et al.* Release of Gas-Phase Halogens by Photolytic Generation of OH in Frozen
717   Halide−Nitrate Solutions: An Active Halogen Formation Mechanism? *The Journal of Physical*
718   *Chemistry A* **114**, 6527-6533, doi:10.1021/jp102072t (2010).

719 35 Ye, C., Zhang, N., Gao, H. & Zhou, X. Photolysis of Particulate Nitrate as a Source of HONO
720   and NOx. *Environmental science & technology* **51**, 6849-6856 (2017).

721 36 Zhao, J., Zhang, Y., Quan, X. & Chen, S. Enhanced oxidation of 4-chlorophenol using sulfate
722   radicals generated from zero-valent iron and peroxydisulfate at ambient temperature. *Separation*
723   *Purification Technology* **71**, 302-307 (2010).

724 37 Wall, K. & Harris, G. Uptake of nitrogen dioxide (NO2) on acidic aqueous humic acid (HA)
725   solutions as a missing daytime nitrous acid (HONO) surface source. *Journal of Atmospheric*
726   *Chemistry* **74**, 283-321 (2017).

727 38 Al-Obaidi, U. & Moodie, R. B. The nitrous acid-catalysed nitration of phenol. *Journal of the*
728   *Chemical Society, Perkin Transactions 2*, 467-472 (1985).

729 39 Paulson, S. E. *et al.* A light-driven burst of hydroxyl radicals dominates oxidation chemistry in
730   newly activated cloud droplets. *Science Advances* **5**, eaav7689, doi:10.1126/sciadv.aav7689
731   (2019).

732 40 Pye, H. O. *et al.* The acidity of atmospheric particles and clouds. *Atmospheric Chemistry Physics*
733   **20**, 4809-4888 (2020).

734 41 Fu, X. *et al.* Persistent heavy winter nitrate pollution driven by increased photochemical oxidants
735   in northern China. *Environmental science & technology* **54**, 3881-3889 (2020).

736 42 Bian, H. *et al.* Investigation of global particulate nitrate from the AeroCom phase III experiment.
737   *Atmospheric Chemistry Physics* **17**, 12911-12940, doi:10.5194/acp-17-12911-2017 (2017).

738 43 Fu, X. *et al.* Anthropogenic emissions of hydrogen chloride and fine particulate chloride in China.
739   *Environmental science & technology* **52**, 1644-1654, doi:10.1021/acs.est.7b05030 (2018).

740 44 Willis, M. D., Leaitch, W. R. & Abbatt, J. P. D. Processes Controlling the Composition and
741   Abundance of Arctic Aerosol. *Reviews of Geophysics* **56**, 621-671, doi:10.1029/2018RG000602
742   (2018).

743 45 Sharma, S. *et al.* A Factor and Trends Analysis of Multidecadal Lower Tropospheric
744   Observations of Arctic Aerosol Composition, Black Carbon, Ozone, and Mercury at Alert,
745   Canada. *Journal of Geophysical Research: Atmospheres* **124**, 14133-14161,
746   doi:10.1029/2019JD030844 (2019).

747 46 Carslaw, K. S., Peter, T. & Clegg, S. L. Modeling the composition of liquid stratospheric
748   aerosols. *Reviews of Geophysics* **35**, 125-154, doi:10.1029/97RG00078 (1997).

749 47 Crutzen, P. J. & Arnold, F. Nitric acid cloud formation in the cold Antarctic stratosphere: a major
750   cause for the springtime 'ozone hole'. *Nature* **324**, 651-655, doi:10.1038/324651a0 (1986).

751   48   Roberts, J. M., Osthoff, H. D., Brown, S. S. & Ravishankara, A. R. N2O5 Oxidizes Chloride to
752   Cl2 in Acidic Atmospheric Aerosol. *Science* **321**, 1059, doi:10.1126/science.1158777 (2008).

753   49   Wexler, A. S. & Clegg, S. L. Atmospheric aerosol models for systems including the ions H+,
754   NH4+, Na+, SO42−, NO3−, Cl−, Br−, and H2O. *Journal of Geophysical Research: Atmospheres*
755   **107**, ACH 14-11-ACH 14-14 (2002).

756   50   Tan, Z. *et al.* Radical chemistry at a rural site (Wangdu) in the North China Plain: observation
757   and model calculations of OH, HO 2 and RO 2 radicals. *Atmospheric Chemistry Physics* **17**, 663-
758   690 (2017).

759   51   Wang, X., Wang, H. & Wang, S. Ambient formaldehyde and its contributing factor to ozone and
760   OH radical in a rural area. *Atmospheric Environment* **44**, 2074-2078 (2010).

761   52   Trebs, I. *et al.* Relationship between the NO2 photolysis frequency and the solar global
762   irradiance. *Atmospheric Measurement Techniques* **2**, 725-739 (2009).

763   53   Xue, L. *et al.* Development of a chlorine chemistry module for the Master Chemical Mechanism.
764   *Geoscientific model development* **8**, 3151-3162 (2015).

765   54   Ammann, M. *et al.* Evaluated kinetic and photochemical data for atmospheric chemistry: Volume
766   VI – heterogeneous reactions with liquid substrates. *Atmospheric Chemistry and Physics* **13**,
767   8045-8228, doi:10.5194/acp-13-8045-2013 (2013).